Single electron multiplication distribution in GEM avalanches

András László,[a,1] **Gergő Hamar,**[a,b] **Gábor Kiss**[a] **and Dezső Varga**[a]

[a]*Wigner Research Centre for Physics, Budapest, Hungary*
[b]*INFN Trieste, Trieste, Italy*

E-mail: laszlo.andras@wigner.mta.hu, hamar.gergo@wigner.mta.hu, kiss.gabor@wigner.mta.hu, varga.dezso@wigner.mta.hu

ABSTRACT: In this paper, measurement results and experimental methodology are presented on the determination of multiplication distributions of avalanches initiated by single electron in GEM foils. The measurement relies on the amplification of photoelectrons by the GEM under study, which is subsequently amplified in an MWPC for signal enhancement and readout. The intrinsic detector resolution, namely the sigma-over-mean ratio of the multiplication distribution is also elaborated. Small gain dependence of the avalanche response distribution is observed in the range of net effective gain of 15 to 100. The distribution has an exponentially decaying tail at large amplitudes. At small amplitudes, the applied working gas is seen to have a well visible effect on the shape of the multiplication distribution. Equivalently, the working gas has an influence on the intrinsic detector resolution of GEMs via suppression of the low amplitude responses. A sigma-over-mean ratio of 0.75 was reached using a neon based mixture, whereas other gases provided an intrinsic detector resolution closer to 1, meaning a multiplication distribution closer to the idealized exponential case.

---

[1]Corresponding author.

Contents

1 Introduction

The intrinsic fluctuation of electron multiplication in avalanche processes of gaseous detectors is an important input parameter at the design phase. An example is the Time Projection Chambers (TPCs) for charged particle trajectory detection, where particle identification is intended to be performed via specific ionization (dE/dx) measurement. The intrinsic energy resolution of the detector, i.e. the magnitude of the gain fluctuation, has direct impact on the dE/dx resolution, and hence on the discrimination power between different particle masses. For the traditionally used Multi Wire proportional Chamber (MWPC) based signal amplification, avalanche fluctuations have been studied long ago [1, 2], revealing a nearly exponential multiplication distribution, meaning a close to 1 intrinsic detector resolution in terms of sigma-over-mean ratio for single electron response.

Avalanche fluctuations are best measured directly, initiated by a single electron. This technique, however, is not trivial in the region of low multiplication, i.e. below gains of $\approx 10^3$. In a work of Zerguerras et al [3, 4] such study was carried out for Micromegas based detectors, revealing a very clear departure from exponential behavior. In the present paper, we experimentally study the electron multiplication processes in GEM [5] based detector.

In the context of the TPC upgrade project [6] of the ALICE experiment at CERN, there is a clear motivation to get access to such fundamental ingredients of gaseous detectors. The results can have impact on the ever improving simulations as well [7]. Earlier studies related to GEM gains and intrinsic resolution of the GEM multiplication process were also reported in [8], however that experimental setting was not aimed at individual avalanche initiation via a single-electron source as in the present paper.

A significant difference of the micropattern based electron multiplication relative to the MWPCs is the constrained avalanche evolution space, which potentially results in a deviation from the idealized exponential avalanche population distribution. Indeed, for Micromegas detectors a significant deviation from the exponential distribution was seen [3, 4], in particular a typical sigma-over-mean ratio significantly smaller than 1 was observed. For GEM based amplification processes, a similar phenomenon is potentially expected. Our experimental setting was designed in order to quantitatively determine the GEM avalanche multiplication distribution and its properties in a wide range of effective gains (about 15 to 100), and in various working gases, with a special emphasis on the low multiplication tail, giving the major contribution to the deviation from the exponential distribution.

The structure of the paper is as follows. In Section 2 the experimental configuration is outlined. Based on this, in Section 3 the ingredients of the formation of the final recorded detector signal in our setting is detailed. In Section 4 a brief discussion is dedicated to the coupling effect between the GEM inefficiency and the true photoelectron yield, which becomes an important detail in the data analysis. In Section 5 the data analysis methods and consistency checks are detailed. In Section 6 the obtained measurement results are reported. In Section 7 a summary is provided.

2   Experimental configuration

The experimental setup is outlined in Fig. 1 and 2, from which one can identify the three sections of the system. First is the "single electron source", second is the actual GEM under study, from which the avalanche is extracted to the third part, the "post-amplifier". A typically observed signal distribution is shown in Fig. 3.

Specifically, a 22 kHz oscillator trigger was used to pulse a UV LED, which released photoelectrons (PEs) from the surface of a gold plated GEM foil inside the working gas volume. The electric potential on the gold plated GEM was configured such that the foil became transparent (effective gain ≈ 1) to the released PEs, thus providing a source of drifting PEs used for the measurements. The mean number of PEs per pulse was variable in the range of about 10^{-2} to 3. After the drift region the conventional GEM foil under study was placed with an effective gain variable in a wide range of about 1 to 100-fold multiplication. Following the GEM foil under study, a high gain stage was realized by an MWPC region, providing further signal enhancement with an electron multiplication up to 300 to 6000.

The readout Front-End Electronics (FEE) and the LED pulser electronics were originally developed for the Leopard project [9]. The FEE was triggered using the same oscillator trigger as for the UV LED, thus providing a zero-bias triggering scheme. The corresponding
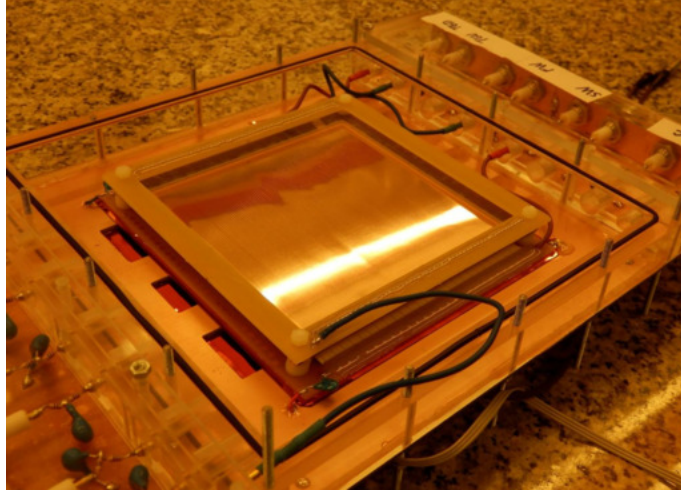
Figure 1. (Color online) Photograph of the chamber of the experimental setup.
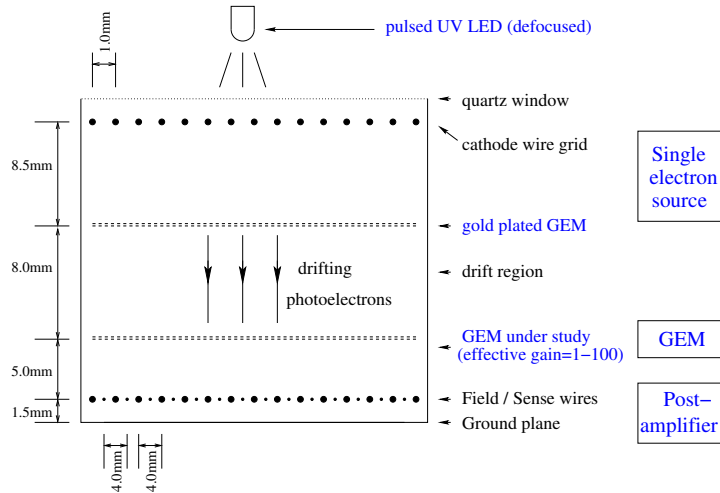

Figure 2. (Color online) Sketch of the full experimental setup. The most important components, namely the pulsed UV LED, the subsequent gold plated GEM as a photoelectron source, the studied amplifier GEM, and the high gain readout stage of an MWPC region is emphasized on the drawing.

trigger delay between the LED and the FEE was adjusted such that the amplified analog signal amplitude was sampled at the signal maximum by the FEE. The MWPC design used the Close-Cathode Chamber (CCC) concept [10, 11] providing a robust amplification region before detection by the FEE. The FEE reading out the Sense Wires delivered the signal amplitude in terms of ADCs, with a gain of about 150 electron/ADC. Typical event statistics from 10^7 pulses for each setting were recorded, therefore the statistical errors of the measurements are negligible and thus are systematics dominated. Various working gases, namely $Ar(80)CO_2(20)$, CH_4, $Ne(90)CO_2(10)$ and $Ne(90)CO_2(10)N_2(5)$ were studied. The pressure of the chamber was atmospheric. The typical drift field was $875\,V/cm$,
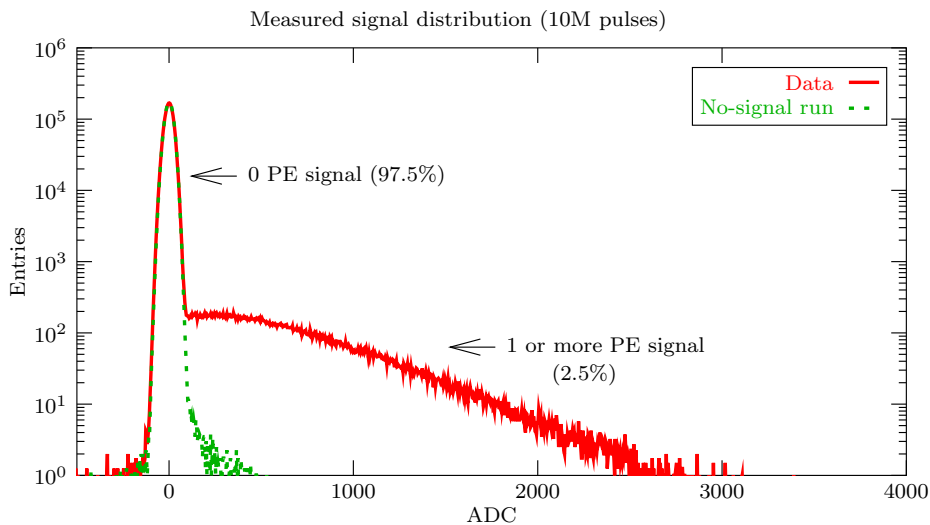
Measured signal distribution (10M pulses)

Figure 3. (Color online) Typical amplitude distribution for UV LED pulses. The peak around zero amplitude corresponds to zero-photoelectron events, whereas the exponential-like tail at larger amplitudes corresponds to the contribution of 1 or more photoelectron events. In the shown example low photoelectron yield was applied, of the order of $2.5 \cdot 10^{-2}$ photoelectron per pulse, and therefore the relative contribution of multi-photoelectron events to the spectrum is negligible. Specifically, the part corresponding to the 1 or more photoelectron response reflects the shape of the 1 photoelectron response distribution, within a systematic error of about a percent. The shown example distribution was recorded in $Ne(90)CO_2(10)$ working gas, at per pulse photoelectron yield of 0.025, GEM gain of 39, and MWPC gain of 2346 in terms of electron multiplication.

whereas the transfer field for extracting the GEM-multiplied electrons was of the order of 800 to 900 V/cm, depending on the particular setting. The studied GEM foil was standard double-mask etched version with a Kapton thickness of $50\,\mu$m and copper thickness of $5\,\mu$m on the two sides. The holes were of the usual double-conical shape with inner diameter of $50\,\mu$m, outer diameter of $70\,\mu$m, and with a pitch of $140\,\mu$m in a hexagonal mesh.

During the data recording runs, special care was taken to make sure that the field on the GEM was stable, and neither the PE yield nor the GEM gain had any drift in time. For this purpose, before the physics runs, special chargeup [12] runs were performed with large PE yield, of the order of 1 PE per pulse, and with large GEM gain, of the order of 50, as well as with large MWPC gain, of the order of 3000. The chargeup runs were continued until the amplitude distribution was seen to be stabilized as a function of time. Additionally, in order to rule out any possibility of a residual drift by the chargeup effects during the physics data taking runs, each physics data taking sequence was performed two times after each-other in order to explicitly verify the time stability of the raw data used in the physics analysis.

3 Signal formation

The three well defined stages of the experimental setup allow to identify a clear relation between the avalanche distribution and the measurable signal. This framework is described in the present section.

3.1 Single electron source

Upon a pulse of the UV LED, PEs are emitted from the top electrode of the upper, gold plated GEM foil. The number of emitted PEs follows a Poisson distribution with an unknown but fixed expectation value for a given setting. The time stability of the UV LED was checked using photomultiplier measurements. The field on the electrodes of the upper, gold plated GEM foil was set in such a way that it became transparent (effective gain ≈ 1), and therefore together with the UV LED the upper, gold plated GEM foil acted as a source of PEs, drifting homogeneously along the drift field as shown in Fig. 2. The distribution of the number n of these PEs are denoted by P_ν, being Poissonian with expectation value ν, i.e.

$$P_\nu(n) = \frac{e^{-\nu}\nu^n}{n!}. \tag{3.1}$$

3.2 Avalanche in the GEM

The PEs reaching the amplifier GEM+MWPC region initiate independent superimposed responses. Therefore, if the amplitude response distribution of the amplifier GEM+MWPC region to a single PE were described by a probability distribution f (that is, the probability of x electrons being detected by the MWPC readout is $f(x)$), then together with the fluctuation of the PE statistics, the probability distribution of the amplitude response x to a single UV LED pulse would be

$$\sum_{n=0}^{\infty} f^{\star(n)}(x)\, P_\nu(n), \tag{3.2}$$

where the symbol $\star$ denotes convolution, and for each non-negative integer n the symbol $f^{\star(n)}$ denotes n-fold convolution of f with itself. In probability theory, a distribution of the form Eq.(3.2) is called a *Poisson compound of f with parameter ν* [13, 14]. The effect of multi-PE contribution can be arbitrarily reduced by making measurements with very low PE yields $\nu \approx 10^{-2}$ in which case only the 0-PE and the 1-PE contribution is relevant. Moreover, in Section 5 we show an advanced method in comparison to the traditional low-PE measurement, which is able to eliminate the multi-PE contribution from a response distribution like Eq.(3.2) in an exact manner, based on Fourier analysis of the Poisson compound.

Due to the presence of the usual additive, approximately Gaussian electronic noise at the input of the FEE amplifier, the observed amplitude distribution can be written as

$$h = g \star \sum_{n=0}^{\infty} f^{\star(n)}\, P_\nu(n), \tag{3.3}$$

where g describes the distribution of the additive electronic noise and h is the final observed amplitude distribution. In practice, experimental determination of g was done in "no-signal" data samples, with having the LED light covered out using a mask. The modification effect of the electronic noise distribution g on the observed distribution h can be reduced by suppressing the additive electronic noise at the FEE input as much as possible, and by increasing the total amplification of the system with respect to the electronic noise level, i.e. with respect to the sigma of g. Moreover, the remaining small residual contribution of the electronic noise may even be fully removed via Fourier based deconvolution, as detailed in Section 5.

3.3 Signals in the post-amplifier

In Eq.(3.3) the probability distribution f describes the common response of the amplifier GEM+MWPC to a single incoming electron. That can be directly related to the distribution of the *effective multiplication response* of the studied GEM to a single incoming electron, being the main object of interest in the present paper, and denoted by p. As such, for a non-negative integer k, the symbol $p(k)$ denotes the probability of the GEM foil to effectively multiply a single incoming electron in such a way that exactly k pieces of multiplied electrons can be extracted by the induction field. With these notations, the distribution f of the GEM+MWPC response x can be written as

$$f(x) = \sum_{k=0}^{\infty} e_\gamma^{\star(k)}(x)\, p(k), \tag{3.4}$$

where e_γ denotes the multiplication response distribution of the MWPC, with a gain γ. Similarly as in Eq.(3.2), for any non-negative integer k the symbol $e_\gamma^{\star(k)}$ denotes k-fold convolution of e_γ with itself. The expression $f(x)$ would mean the probability of x electrons to be read out from the GEM+MWPC system, given a single incoming electron. Similarly, the symbol $e_\gamma(x)$ would mean the probability of x electrons to be read out from the MWPC, given a single electron entering the MWPC region. In consequence, $e_\gamma^{\star(k)}(x)$ is the probability of x electrons to be read out from the MWPC, given that k electrons entered the MWPC region. The model Eq.(3.4) is suggested by the idea that the MWPC avalanches triggered by the extracted GEM-multiplied electrons evolve independently. This is justified by the applied relatively low MWPC gains (about $\gamma \approx 300$ to 3500 in terms of electron multiplication) and by the relatively low number of MWPC-amplified incoming electrons (GEM gains of the order of 1 to 100).

The Leopard FEE [9] used for the signal readout from the Sense Wires included a preamplifier, having a total gain of 1 ADC for about 150 electrons. Since the studies performed in the paper needed a relatively large dynamical range in terms of measured amplitudes, a careful study was performed to check and compensate any possible nonlinearities of the FEE preamplifier when approaching the saturation range. This is also detailed in Section 5.

In the list below the possible contributions of all the known detector effects are summarized which can turn up as ingredients in the observed amplitude distribution for single

UV LED pulses.

1. Photoelectron statistics fluctuations P_ν.

2. GEM effective multiplication fluctuations p, being the main object of interest of the study presented in the paper.

3. MWPC multiplication fluctuations e_γ.

4. Additive electronic noise fluctuations g at the input of the FEE.

5. A possible deterministic non-linearity transfer function of the FEE amplifier, due to the wide dynamic range of the study.

6. Pedestal shift and subsequent AD conversion.

In Section 5 the methodologies for quantification and correction for the above effects are detailed, in order to obtain measurements for the GEM effective multiplication distribution p with the lowest possible systematic errors.

4 Coupling effect between detection inefficiency and photoelectron yield

In this section a brief probability theory argument is presented, showing that the true PE yield and the GEM inefficiency cannot be disentangled, i.e. it is not possible to know a priori whether a close-to-zero amplitude was detected because no PE was emitted by a given LED pulse, or some PEs were present in the system, but the corresponding GEM response was lost due to an intrinsic inefficiency effect. The argument shows that the system with possible GEM inefficiencies can, however, be uniquely characterized by an effective PE yield, being the product of the GEM efficiency and of the true PE yield. An inefficiency effect, i.e. a high value for $f(0)$, can appear for instance when the PE is lost due to attachment in the gas [15], which can be caused by electronegative gas contamination.

Let us introduce the definition

$$\tilde{p}(k) = \frac{1}{1 - p(0)} \left(1 - \delta_{0\,k}\right) p(k) \tag{4.1}$$

for all non-negative integers k, where $\delta_{0\,k}$ denotes the Kronecker delta of index $0, k$. Since $p(0)$ is the probability of extracting 0 electrons from the amplifier GEM foil, i.e. the *GEM inefficiency*, $\tilde{p}$ is the conditional probability distribution of the number of extracted GEM-multiplied electrons with the condition of extracting at least 1 electron. This quantity, i.e. the distribution of the *net effective multiplication*, excludes the GEM inefficiency $p(0)$. Using such notation, one has the identity

$$p(k) = p(0)\,\delta_{0\,k} + (1 - p(0))\,\tilde{p}(k) \tag{4.2}$$

for all non-negative integers k. The splitting Eq.(4.2) may also be realized at the level of amplification by the combined GEM+MWPC stage, namely with the definition

$$\tilde{f}(x) = \sum_{k=0}^{\infty} e_\gamma^{\star(k)}(x)\, \tilde{p}(k) \tag{4.3}$$

one has the identity

$$f(x) = p(0)\, \delta(x) + (1 - p(0))\, \tilde{f}(x), \tag{4.4}$$

where δ denotes the Dirac delta, and x is the amplitude response. It is seen that $\tilde{f}$ is the conditional multiplication distribution of the GEM+MWPC system with the condition that at least 1 electron was extracted from the GEM foil. That is, $\tilde{f}$ is almost the same as f, except that the GEM inefficiency $p(0)$ is not counted within. Note that $\tilde{f}$ can be re-expressed as

$$\tilde{f}(x) = \frac{1}{1 - p(0)} \sum_{k=1}^{\infty} e_\gamma^{\star(k)}(x)\, p(k). \tag{4.5}$$

From such an alternative representation it is seen that $\tilde{f}$ can be considered as a regular probability density function of the continuous variable x, since the singular Dirac delta contribution within f is excluded from $\tilde{f}$, and because the MWPC multiplication response distribution function e_γ behaves like a regular probability density function of a continuous variable above the applied MWPC gains larger than $\gamma \approx 300$. As a consequence of Eq.(3.3), Eq.(3.1) and the convolution theorem [16, 17], in Fourier space one has the identity

$$
\begin{aligned}
H &= G \sum_{n=0}^{\infty} F^n \frac{e^{-\nu} \nu^n}{n!} \\
&= G \, \exp\left(-\nu\,(1 - F)\right) \\
&= G \, \exp\left(-\,(1 - p(0))\,\nu\,\left(1 - \tilde{F}\right)\right),
\end{aligned} \tag{4.6}
$$

where F, $\tilde{F}$, G, H are the Fourier transforms of the probability density functions f, $\tilde{f}$, g, h, respectively. Motivated by Eq.(4.6), the *effective photoelectron yield*

$$\nu_{\text{eff}} = (1 - p(0))\, \nu, \tag{4.7}$$

is introduced, which is the true PE yield ν multiplied by the GEM efficiency $1 - p(0)$. With that, the identity

$$H = G \, \exp\left(-\nu_{\text{eff}}\left(1 - \tilde{F}\right)\right) \tag{4.8}$$

follows, which after an inverse Fourier transformation yields an alternative form of Eq.(3.3):

$$h = g \star \sum_{n=0}^{\infty} \tilde{f}^{\star(n)} P_{\nu_{\text{eff}}}(n).$$

(4.9)

This identity explicitly shows that in our setting the GEM inefficiency and the PE yield cannot be disentangled, but a configuration can still be characterized by the effective PE yield ν_{eff}, and by the net effective multiplication distribution $\tilde{p}$ and $\tilde{f}$ of the GEM and the GEM+MWPC system. Our analysis will thus aim to characterize the net effective GEM multiplication distribution $\tilde{p}$.

5   Analysis, calibration and data consistency

In each given setting, the distribution of the amplitude response to single UV LED pulses in terms of ADCs were recorded. The processes involved in the formation of the ADC signal is described in Section 3 and Section 4. In this section the analysis procedures, used for correction or quantification of those detector effects are detailed step-by-step.

5.1   Pedestal shift and electronic noise quantification

The zero point of the AD converter of the FEE is determined via special no-signal pedestal runs, with the light from the UV LED blocked. Using the pedestal value, the observed amplitude distributions were corrected such that zero signal corresponds to zero ADC. The pedestal runs also provide measurements on the electronic noise fluctuations, i.e. on the probability density function g appearing in Eq.(3.3) and Eq.(4.9). Typically, g turned out to be an approximately Gaussian distribution with a standard deviation of the order of 20 ADCs.

5.2   FEE non-linearity characterization

For accurate determination of the 1-PE response distribution $\tilde{f}$ (or $\tilde{p}$), a large dynamical range is needed in order to simultaneously resolve the exponential-like tail at large amplitudes and a possible deviation from exponential at low amplitudes. Motivated by this, the linearity of the FEE was carefully checked by several independent methods. The most accurate method was the *method of percentiles*: amplitude response distributions were recorded with all the settings fixed except for the MWPC gain (controlled by the Sense Wire voltage). In such a scenario the true amplitude response distributions have the same shapes for all the configurations up to a scale factor by the relative change of the MWPC gain. A deviation from such behavior can be accounted to the FEE non-linearity, and can directly be used for an accurate determination of the necessary non-linearity correction function throughout the entire dynamical range. The accuracy of the non-linearity compensation can be checked by further independent measurements using different MWPC gain settings. A residual systematic deviation of 0.5% from linearity was observed after the applied non-linearity compensation. The linearity after the compensation was also validated using direct charge deposition on the Sense Wires. For charge deposition, a pulsed current generator

was applied for a fixed time duration, and the corresponding ADC value was recorded. The results of this validation is shown in Fig. 4, and very good linearity is seen. This test, however, is less accurate in comparison to the method of percentiles, due to the systematic uncertainty on the control of the deposited charges, being not worse than 5% in relative accuracy. The direct charge measurement, however, readily provides the FEE gain in terms of charge over ADC. The measured FEE gain was seen to be 142.3 ± 7(syst.) electrons/ADC.
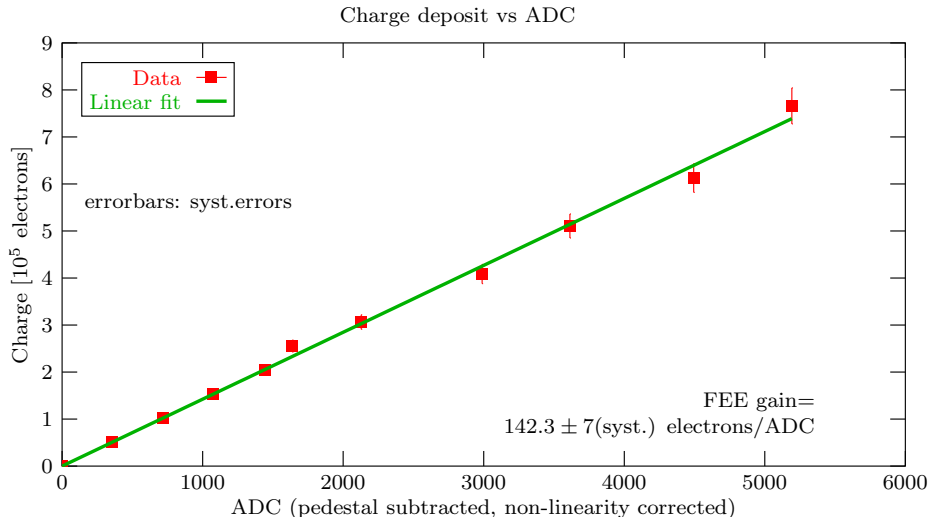

Figure 4. (Color online) Deposited charge versus the corresponding ADC. The measurement was performed using a test pulser delivering a well defined amount of charge on the Sense Wires. The shown ADC values are already pedestal subtracted and non-linearity corrected with the described method. Good linearity is seen in the entire dynamical range. The deposited test charge values carry approximately 5% systematic errors. This pulser test also provides the value of the FEE gain in terms of electron count to ADC conversion, being 142.3 ± 7(syst.) electrons/ADC.

From this point on, if not otherwise stated, both pedestal subtraction and non-linearity compensation is always applied to the ADC scales throughout the paper.

5.3 Elimination of multi-PE contribution

Due to the identity Eq.(4.9), the observed amplitude distributions have contributions from 0-PE events with a weight of $e^{-\nu_{\mathrm{eff}}}$, from 1-PE events with a weight of $e^{-\nu_{\mathrm{eff}}} \nu_{\mathrm{eff}} = O\left(\nu_{\mathrm{eff}}\right)$, and multi-PE events with a total weight of $1 - e^{-\nu_{\mathrm{eff}}}\left(1 + \nu_{\mathrm{eff}}\right) = O\left(\nu_{\mathrm{eff}}^2\right)$. The contamination by the multi-PE events within the sample of 1 or more PE events has thus a dependency of $\frac{1 - e^{-\nu_{\mathrm{eff}}}\left(1 + \nu_{\mathrm{eff}}\right)}{e^{-\nu_{\mathrm{eff}}} \nu_{\mathrm{eff}}} = O(\nu_{\mathrm{eff}})$. Therefore, the most commonly applied method, as also done e.g. in [3, 4], is to take measurements with very low effective PE yield $\nu_{\mathrm{eff}} \leq 10^{-2}$, in which case the multi-PE component of the amplitude distribution h becomes dominated by the 1-PE yield within a systematic error of 0.5%. The simplicity of this approach makes that method a good experimental reference, however, as e.g. seen in the bottom panel of Fig. 2 the separation of the 0-PE and 1-PE response distributions is not a trivial task due to their substantial overlap.

A possible way to disentangle the 0-PE and the 1-PE contribution is to fit a model of the form Eq.(4.9) to the observed amplitude distribution h, with some parametric model for the 1-PE distribution $\tilde{f}$, such as a Gamma distribution of the form $1/\left(s\,\Gamma\left(\kappa\right)\right)\left(x/s\right)^{\kappa-1}\mathrm{e}^{-x/s}$ for the response amplitudes x. The Gamma distribution is the continuous analogy of Pólya distribution, often used in parametrization of avalanche responses. Here Γ denotes the Gamma function, s is the slope parameter and the parameter κ measures the deviation from exponential, namely the sigma-over-mean ratio of such Gamma distribution is $1/\sqrt{\kappa}$. This kind of model fit based analysis is shown in Fig. 5. The data is seen to be very well described by the Gamma distribution for the 1-PE response distribution $\tilde{f}$. The fit also leads to an accurate estimate for the effective PE yield ν_{eff}.
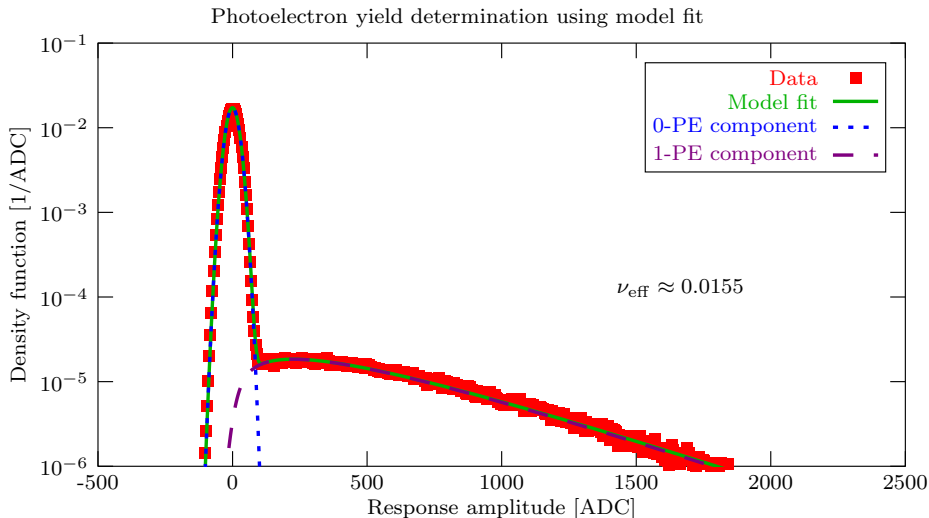

Figure 5. (Color online) Disentangling of the 0-PE and the 1-PE contribution to the amplitude distribution via model fit. A parametric Gamma distribution shape is assumed for the true 1-PE response distribution $\tilde{f}$. The model describes the measured distribution very well. The fit procedure also quantifies the effective PE yield ν_{eff}. The shown example was recorded in $\mathrm{Ne(90)CO_2(10)}$ working gas, at per pulse effective PE yield of 0.0155, GEM gain of 39, and MWPC gain of 2346 in terms of electron multiplication.

The model fit method, although it helps to reduce the systematic error in the PE yield estimation, brings in a slight model dependence, especially at the low amplitude region of the distribution. This can be reduced by recording the response distribution h in several copies with all the settings fixed except for the MWPC gain. In that case, the overlap of the low amplitude region of the 1-PE response with the electronic noise peak of the 0-PE response can be significantly reduced. This procedure is possible due to the presence of the second amplification stage by the MWPC zone. Such a study is shown in Fig. 6, which helps to experimentally get closer to the low amplitude region of the 1-PE response distribution.

A model independent study of the low amplitude region of the 1-PE response $\tilde{f}$ at simultaneously fixed effective PE yield, GEM gain and MWPC gain can be performed using Eq.(4.8). That identity allows one to reconstruct the Fourier spectrum $\tilde{F}$ of the 1-
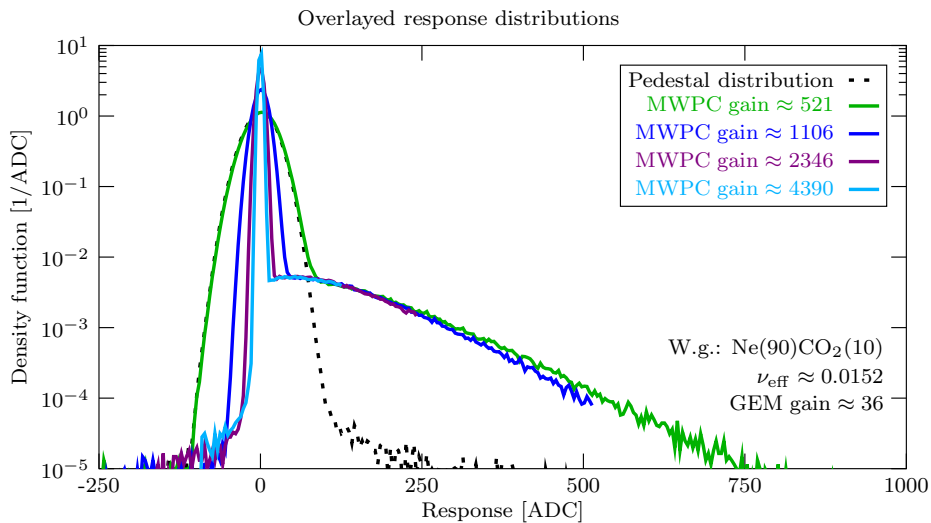
Overlayed response distributions

Figure 6. (Color online) Disentangling of the 0-PE and the 1-PE contribution via MWPC gain scan and subsequent overlaying of amplitude distributions after rescaling with the relative MWPC gains of the settings. Due to the scan in the gain of the final amplifier stage, the MWPC, the low amplitude region can be better disentangled from the 0-PE peak, determined by the electronic noise distribution. The shown example was recorded in $Ne(90)CO_2(10)$ working gas, at per pulse effective PE yield of 0.0152, GEM gain of 36, and MWPC gain of 521 to 4390 in terms of electron multiplication.

PE response distribution $\tilde{f}$, given the Fourier spectrum H of the total observed amplitude distribution h, the Fourier spectrum G of the electronic noise distribution g, and the effective PE yield ν_{eff} via the formula:

$$\tilde{F} = 1 + \frac{1}{\nu_{\text{eff}}} \ln\left(\frac{H}{G}\right). \tag{5.1}$$

After an inverse Fourier transformation, this delivers the 1-PE distribution of interest $\tilde{f}$ without model assumptions. Since h, H, g, G can be determined from experimental data the only unknown for the procedure to work is the effective PE yield ν_{eff}. Given that, the multi-PE contribution can be factorized in an exact manner via Eq.(5.1) at any PE yield, in particular also at the large PE yield limit. Clearly, an increased effective PE yield ν_{eff} improves the signal to noise ratio, thus the task remains to determine ν_{eff} from the amplitude distribution h at large PE yields in a reliable way. That can be done via the Riemann-Lebesgue lemma [18], which states that the Fourier spectrum of every probability density function of a continuous variable, in particular $\tilde{F}$, decays to zero at infinite frequencies. As a consequence of that and of Eq.(4.8), one has the identity

$$\lim_{|\omega| \to \infty} \frac{H(\omega)}{G(\omega)} = e^{-\nu_{\text{eff}}} \tag{5.2}$$

which can be used for determination of the effective PE yield ν_{eff} from the asymptotics

of the ratio of the Fourier spectrum H of the amplitude distribution h and of the Fourier spectrum G of the electronic noise distribution g. The identity Eq.(5.2) is illustrated in Fig. 7. It is seen that the ratio H/G of the Fourier spectra relaxes to a constant value, $\mathrm{e}^{-\nu_{\mathrm{eff}}}$, at the asymptotics, thus determining the effective PE yield ν_{eff}. The asymptotic region used for the determination of $\mathrm{e}^{-\nu_{\mathrm{eff}}}$ via fit was defined to be a $|\text{frequency}| \geq 34\,\sigma$ sideband. Here $\sigma = 1/(2\pi\,(\sigma_h^2 - \sigma_g^2)^{1/2})$ is a lower estimate of the standard deviation of the non-noise component of the Fourier spectrum, in which σ_h and σ_g denotes the standard deviation of the distributions h and g, respectively. After the determination of the value of ν_{eff}, the Fourier spectrum $\tilde{F}$ of the pure 1-PE response $\tilde{f}$ can be determined via the formula Eq.(5.1), which is shown in Fig. 8. The reconstructed pure 1-PE response distribution $\tilde{f}$ can then be obtained via an inverse Fourier transformation. For the Fourier transformations, the FFT implementation of GSL [19] was used. The resulting reconstructed 1-PE response distribution is shown in Fig. 9. For cross-check purposes it is overlayed with the direct measurement using the MWPC gain scan method shown previously in Fig. 6. Good consistency is seen between the two independent approach. The advantage of the Fourier based Poisson compound decomposition method is the complete elimination of the overlap region with the electronic noise of the 0-PE contribution and thus the extrapolation uncertainty to small amplitudes is not present anymore.
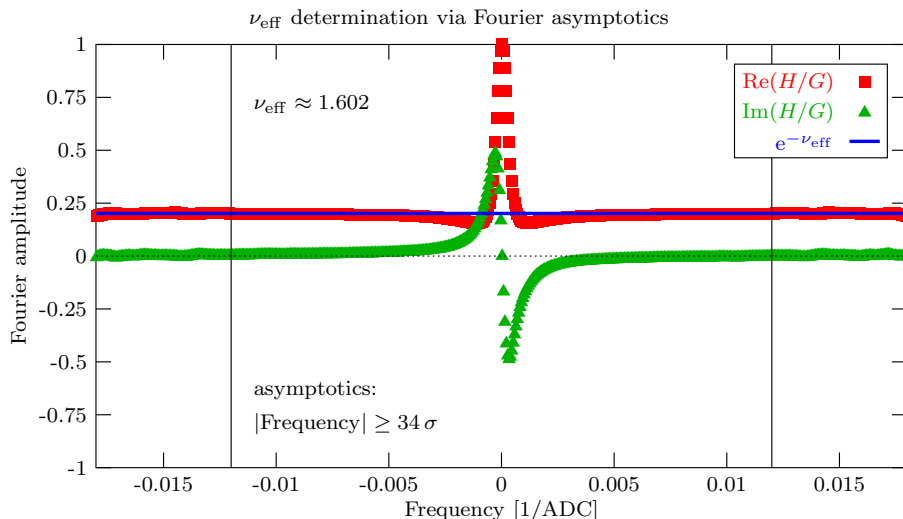

Figure 7. (Color online) Experimental determination of the effective PE yield ν_{eff} using Fourier based Poisson compound decomposition method. The asymptotic value of the Fourier spectrum ratio H/G of the amplitude and noise distributions relaxes to $\mathrm{e}^{-\nu_{\mathrm{eff}}}$ by means of Eq.(5.2). The asymptotic region for fitting the constant $\mathrm{e}^{-\nu_{\mathrm{eff}}}$ model to the data was a sideband of $|\text{frequency}| \geq 34\,\sigma$, shown by the vertical lines. The shown example was recorded in $\mathrm{Ne}(90)\mathrm{CO}_2(10)$ working gas, at per pulse effective PE yield of 1.602, GEM gain of 36, and MWPC gain of 1106 in terms of electron multiplication.

A further possibility of the elimination of the multi-PE contribution in a model independent way is performing the analysis at the level of moments. An idealized avalanche process is self-similar, i.e. the conditional probability density above any multiplication threshold is
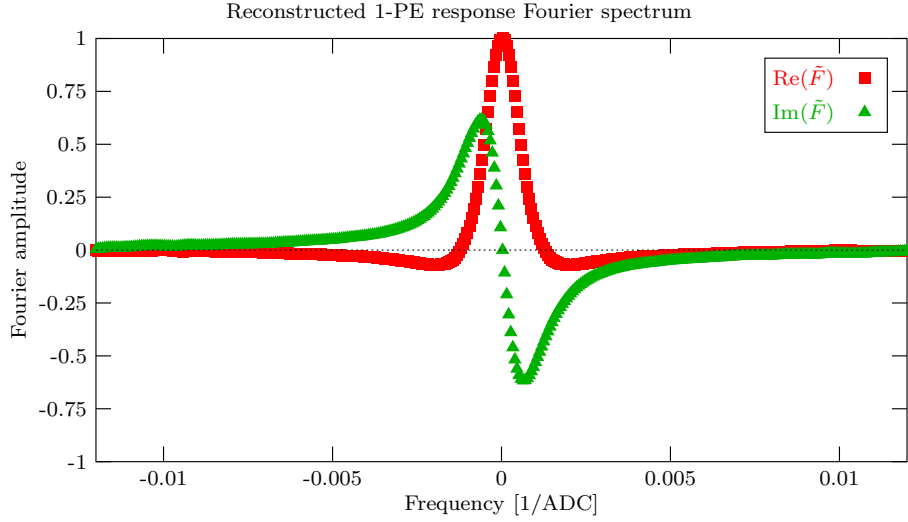
Figure 8. (Color online) Experimental determination of the Fourier spectrum $\tilde{F}$ of the pure 1-PE response distribution $\tilde{f}$ via Eq.(5.1). The shown example was recorded in Ne(90)CO$_2$(10) working gas, at per pulse effective PE yield of 1.602, GEM gain of 36, and MWPC gain of 1106 in terms of electron multiplication.
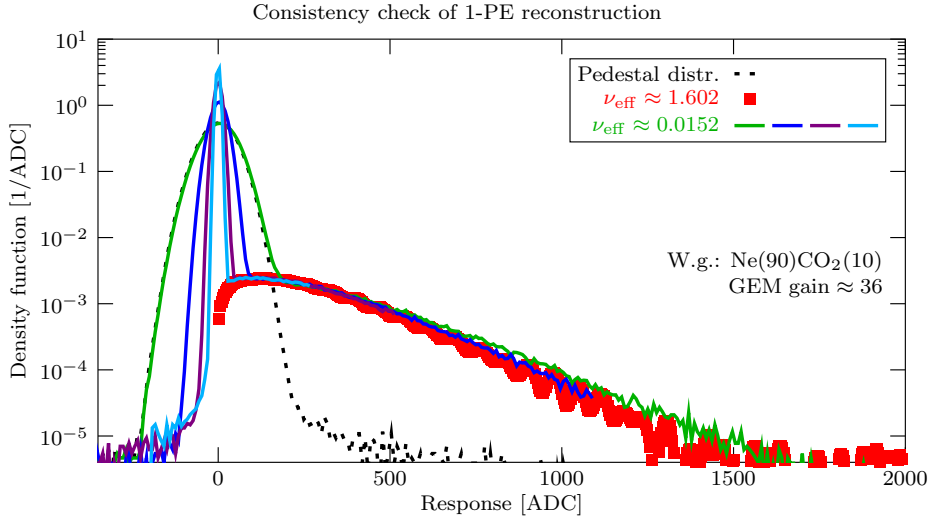

Figure 9. (Color online) Experimental determination of the pure 1-PE response distribution $\tilde{f}$ via Poisson compound decomposition method in Fourier space. For cross-check purposes, the more direct measurement using MWPC gain scan is also overlayed on the figure, and good agreement is seen. The shown example was recorded in Ne(90)CO$_2$(10) working gas, at per pulse effective PE yield of 1.602, GEM gain of 36, and MWPC gain of 1106 in terms of electron multiplication.

the same as the full multiplication distribution, which implies that it is exponential. An exponential distribution has an important property: its sigma-over-mean ratio is 1. A distribution deviating from the exponential, e.g. a Gamma distribution, has a sigma-over-mean

slightly different than that of 1. Therefore, the sigma-over-mean ratio of the 1-PE distribution provides important information about a deviation from the idealized exponential case. Due to the Poisson compound nature Eq.(4.9) of the observed amplitude distribution h, one has the identity

$$\begin{aligned} \mu_h &= \mu_g + \nu_{\text{eff}}\,\mu_{\tilde{f}}, \\ \sigma_h^2 &= \sigma_g^2 + \nu_{\text{eff}}\left(\sigma_{\tilde{f}}^2 + \mu_{\tilde{f}}^2\right), \end{aligned} \tag{5.3}$$

where μ_h, σ_h, μ_g, σ_g, $\mu_{\tilde{f}}$, $\sigma_{\tilde{f}}$ denote the mean and standard deviation of the distributions h, g and $\tilde{f}$, respectively. That leads to the equation

$$\frac{\sigma_{\tilde{f}}}{\mu_{\tilde{f}}} = \sqrt{\nu_{\text{eff}}\,\frac{\sigma_h^2 - \sigma_g^2}{(\mu_h - \mu_g)^2} - 1} \tag{5.4}$$

for the sigma-over-mean ratio of the 1-PE response distribution $\tilde{f}$. It is seen that solely by determining the effective PE yield ν_{eff}, the sigma-over-mean ratio of the 1-PE amplitude response distribution $\tilde{f}$ can simply be reconstructed just from the first two statistical moment of the amplitude distribution h and of g. The results of such statistical moment based analysis shall also be presented in Section 6.

5.4 Elimination of the MWPC response contribution

The true motivation of the present study is to measure the GEM response distribution, for which reason an unfolding procedure has been developed to eliminate the MWPC contribution from the measured GEM+MWPC signal. This correction is seen to be small, and can be performed both at the level of response distributions or at the level of moments, i.e. specifically for the sigma-over-mean ratios.

The 1-PE amplitude response distribution of the GEM and the GEM+MWPC system is related via Eq.(4.3). It shall be shown that the shape modification effect by the MWPC stage is suppressed with increased GEM gain, and is rather small above gains of ≈ 10. This is because for large k, the distribution $e_\gamma^{\star(k)}$ in Eq.(4.3) approximates a narrow Gaussian with mean $k\,\gamma$ and standard deviation $\sqrt{k}\,\sigma_{e_\gamma}$, i.e. following the shape of the weight $\tilde{p}$ accurately for large k. Moreover, the shape modification effect of the MWPC can be corrected in an exact manner, as shall be shown in the following.

In order to quantify the effect of shape modification of the GEM response by the MWPC stage, one should note that the 1-electron amplitude response distribution e_γ of the MWPC is of exponential type to a good accuracy [1, 2] at gains of the order of 10^2 to 10^4. This is quite expected due to the large number of avalanche generations in the MWPC multiplication process, which tends to shift the avalanche evolution closer toward idealized avalanches. The close to exponential nature of MWPC response distributions is also confirmed by our control measurements. In such control runs we set the amplifier GEM foil to transparent (effective GEM gain ≈ 1), recorded the amplitude distribution with large PE yield, of the order of 1 to 3 PE per pulse in order to compensate the missing GEM gain in the signal to noise ratio. Then, with the method of moments described previously, the

sigma-over-mean ratio for the 1-electron response was estimated via the formula Eq.(5.4). That estimate resulted in 0.922 ± 0.05(syst.) at typical settings, being rather close to the idealized exponential having sigma-over-mean ratio of 1. Moreover, the fit of convolution of the Gaussian noise model with the Poisson compound of an exponential 1-PE response distribution of the MWPC system describes the MWPC-only data very well, as shown in Fig. 10 for a typical setting. Thus, an approximation of e_γ with exponential distribution having slope parameter γ is well justified.
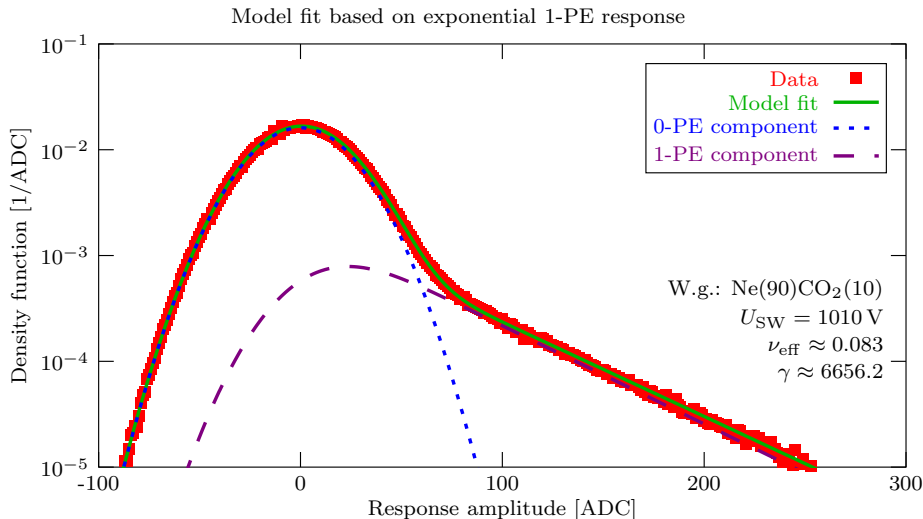

Figure 10. (Color online) Model fit to MWPC-only amplitude distribution in a typical setting. The used model assumed of the form Eq.(4.9) with the 1-PE response distribution $\tilde{f}$ taken here to be of purely exponential type, and the noise distribution g being a Gaussian distribution measured from pedestal runs. Apparently, the exponential model for the 1-PE distribution describes the data well. The shown data set was recorded in $Ne(90)CO_2(10)$ working gas, at net effective PE yield $\nu_{\text{eff}} \approx 0.083$ and at $\gamma \approx 6656.2$ MWPC gain in terms of electron multiplication, corresponding to $U_{\text{SW}} = 1010\,\text{V}$ potential on the Sense Wires.

The effect of the shape modification by the MWPC stage in terms of Eq.(4.3) is illustrated by a simulation shown in Fig. 11, assuming the 1-PE GEM response to be some Gamma distribution, and e_γ to be of exponential type. The top panel shows that the effect may not be negligible for small effective GEM gains, whereas in the bottom panel it is seen that the shape distortion effect by the MWPC stage for larger GEM gain settings is negligible.

Whenever the shape distortion effect by the MWPC is not considered to be fully negligible, it may be corrected for in an exact manner using unfolding. That is because Eq.(4.3) reflects that $\tilde{f}$ is nothing but $\tilde{p}$ folded with a response function of the form $\rho_\gamma(x|k) = e_\gamma^{\star(k)}(x)$ for non-negative integers k and amplitude values x. That kind of transformations can be inverted using unfolding methods such as [20–22]. The pertinent response function is illustrated in Fig. 12 as well as the result of the iterative unfolding by the method [20–22].

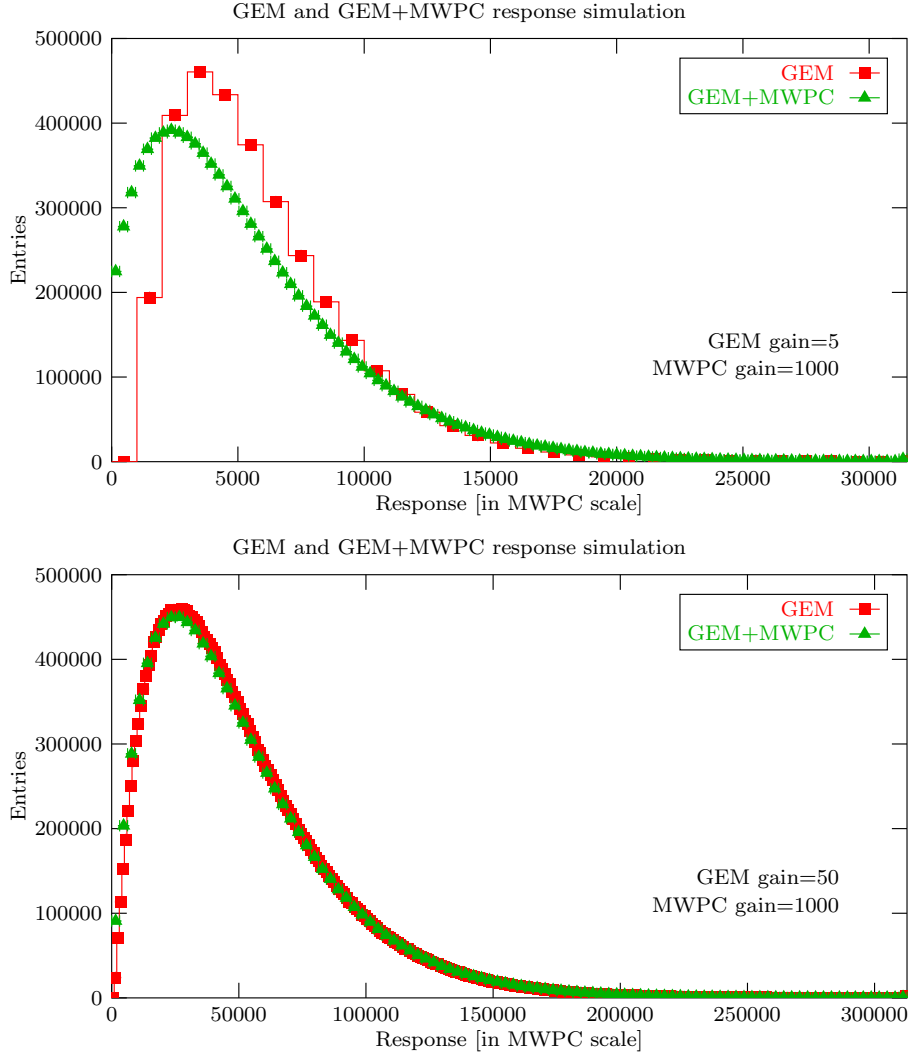The effect of the MWPC response can also be removed at the level of moments. Namely,

Figure 11. (Color online) Top panel: a simulation example in order to demonstrate the shape distortion effect of the MWPC response at net GEM effective gain = 5. Bottom panel: the same with net GEM effective gain = 50. It is seen that the shape distortion is negligible at the higher GEM gain setting. The hypothetical GEM amplitude distribution was assumed to be a Gamma distribution in both cases, with $\kappa = 2$.

because of Eq.(4.3), the identity

$$
\begin{aligned}
\mu_{\tilde{f}} &= \mu_{e_\gamma}\,\mu_{\tilde{p}}, \\
\sigma_{\tilde{f}}^2 &= \sigma_{e_\gamma}^2\,\mu_{\tilde{p}} + \mu_{e_\gamma}^2\,\sigma_{\tilde{p}}^2
\end{aligned}
\tag{5.5}
$$

follows, where $\mu_{\tilde{f}}$, $\sigma_{\tilde{f}}$, μ_{e_γ}, σ_{e_γ}, $\mu_{\tilde{p}}$, $\sigma_{\tilde{p}}$ denote the mean and standard deviation of the distributions $\tilde{f}$, e_γ and $\tilde{p}$, respectively. Taking into account that by definition one has
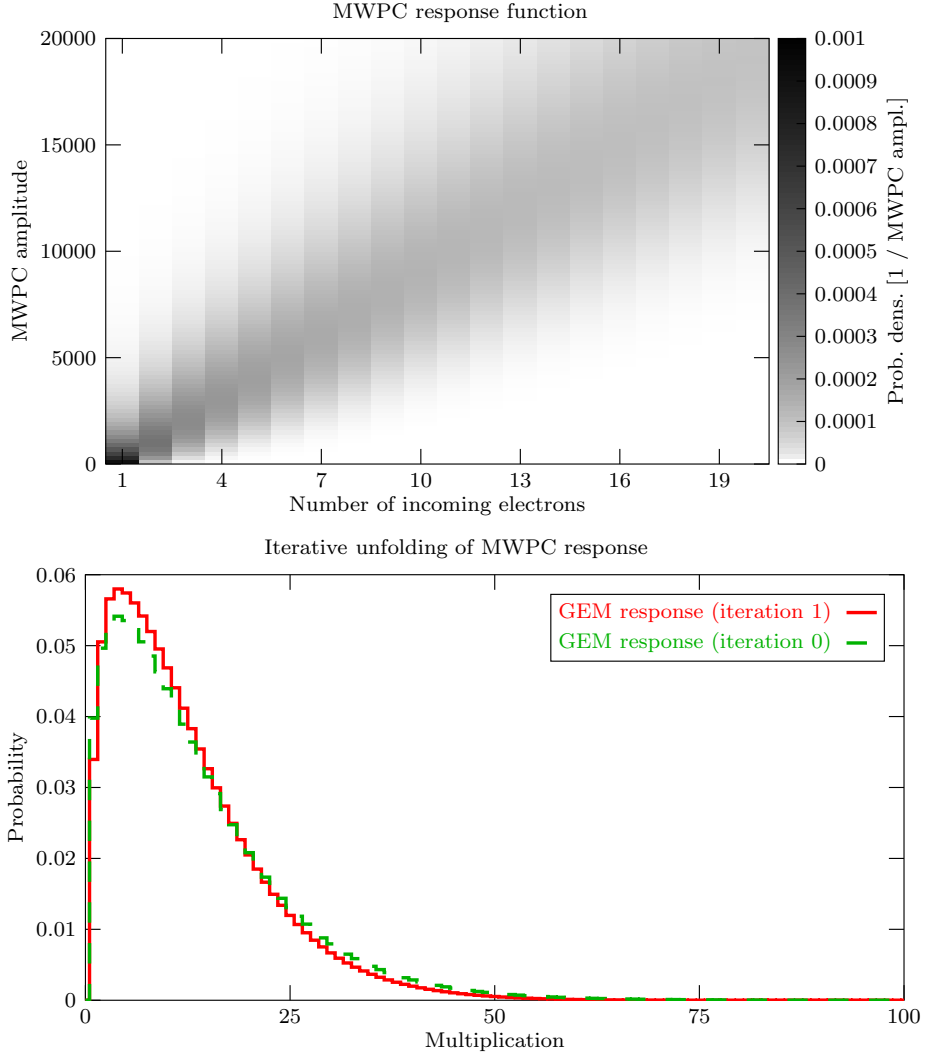
Figure 12. (Color online) Top panel: the response function of the MWPC amplification stage. Bottom panel: the result of the iterative unfolding method [20–22] for the removal of the MWPC response function from the amplitude distribution. The method already converges in one iteration, and the corresponding correction is seen to be very small. The shown data was recorded in $Ne(90)CO_2(10)$ working gas, at GEM gain 12, and MWPC gain 3015 in terms of electron multiplication.

$\mu_{e_\gamma} = \gamma$, the expression

$$\frac{\sigma_{\tilde{p}}}{\mu_{\tilde{p}}} = \sqrt{\left(\frac{\sigma_{\tilde{f}}}{\mu_{\tilde{f}}}\right)^2 - \left(\frac{\sigma_{e_\gamma}}{\mu_{e_\gamma}}\right)^2 \frac{\gamma}{\mu_{\tilde{f}}}} \tag{5.6}$$

follows for the sigma-over-mean ratio of the 1-electron net GEM multiplication distribution $\tilde{p}$. From the right hand side it is seen that the correction for the contribution of the MWPC response is suppressed by 1 / GEM gain, i.e. by $1/\mu_{\tilde{p}} = \gamma/\mu_{\tilde{f}}$. This quantitatively

demonstrates the phenomenon that the MWPC response does not significantly distort the shape of the GEM distribution at GEM gains larger than about 10. Putting together the formula Eq.(5.4) and Eq.(5.6), one arrives at

$$\frac{\sigma_{\tilde{p}}}{\mu_{\tilde{p}}} = \sqrt{\nu_{\mathrm{eff}} \, \frac{\sigma_h^2 - \sigma_g^2}{(\mu_h - \mu_g)^2} - \left(\frac{\sigma_{e_\gamma}}{\mu_{e_\gamma}}\right)^2 \frac{\nu_{\mathrm{eff}} \, \gamma}{\mu_h - \mu_g} - 1},$$

(5.7)

which can further be simplified using $\sigma_{e_\gamma}/\mu_{e_\gamma} \approx 1$. In summary: the sigma-over-mean ratio of the 1-electron GEM response can be experimentally determined via measuring μ_h, σ_h, μ_g, σ_g, ν_{eff} and γ in a given setting. The result of such moment based analysis shall also be shown in Section 6.

5.5 Estimation of GEM and MWPC gains

For the interpretation of the obtained results, estimation of GEM gain $\mu_{\tilde{p}}$ in a given setting is necessary. Also, as shown previously, for the corrections for the MWPC effects having an estimate for the MWPC gain γ is also needed. For an estimation procedure, the identity

$$\mu_h - \mu_g = \nu_{\mathrm{eff}} \, \gamma \, \mu_{\tilde{p}}$$

(5.8)

is the starting point, which means that by measuring μ_h, μ_g and ν_{eff}, the combined GEM+MWPC gain $\gamma \, \mu_{\tilde{p}}$ is readily available. Our procedure was to obtain calibration curve of the MWPC gain γ as a function of Sense Wire voltage in order to calculate $\mu_{\tilde{p}}$ from the combined gain $\gamma \, \mu_{\tilde{p}}$ in a given setting.

The calibration of the MWPC gain γ was implemented in two steps. First, the Sense Wire voltage dependence of γ was quantified. This was done by setting the amplifier GEM foil to a large gain, of the order of net effective multiplication 50, and by setting a large PE yield, of the order of 1 PE per pulse. Then, a Sense Wire voltage scan was performed. Because of Eq.(5.8), the shape of the Sense Wire voltage dependence of the MWPC gain could be determined since ν_{eff} and $\mu_{\tilde{p}}$ was kept constant. Given the shape of the Sense Wire voltage dependence of the MWPC gain γ, its absolute normalization was then obtained in a setting with transparent GEM (effective gain ≈ 1), large PE yield (≈ 1), and a large Sense Wire voltage setting using the identity

$$\frac{\sigma_h^2 - \sigma_g^2}{\mu_h - \mu_g} = \frac{\sigma_{\tilde{f}}^2 + \mu_{\tilde{f}}^2}{\mu_{\tilde{f}}}$$

(5.9)

which follows from Eq.(5.3), where in the present situation one has $\tilde{f} = e_\gamma$ since the GEM did not amplify in such calibration runs. Note that the PE yield ν_{eff} cancels in Eq.(5.9). Using now $\gamma = \mu_{e_\gamma}$ and $\sigma_{e_\gamma}/\mu_{e_\gamma} \approx 1$, the absolute MWPC gain can be estimated via the formula

$$\gamma \approx \frac{1}{2} \frac{\sigma_h^2 - \sigma_g^2}{\mu_h - \mu_g}$$

(5.10)

in such calibration setting. Note that due to the lower signal to noise ratio without the GEM amplification, such absolute calibration runs were only possible at larger PE yields and at larger MWPC gain settings in order to maintain a good signal to noise ratio. The compatibility of the Sense Wire voltage dependence of the absolute MWPC gain values were cross-checked with the relative calibration curve of the MWPC gain in a couple of extremal settings at large PE yield and large MWPC gain. The result of the MWPC gain calibration procedure is shown in Fig. 13. After the MWPC calibration procedure, the net effective GEM gain can always be calculated in a given setting via Eq.(5.8). The obtained net effective GEM gain curves are shown in Fig. 14. It is seen that in the region $\Delta U_{\mathrm{GEM}} \approx 10 - 90\,\mathrm{V}$ the net effective GEM gains are ≈ 1 in all the working gases, i.e. the GEM foil becomes transparent to electrons and no multiplication takes place. In our experimental runs the transparent setting was thus defined as $\Delta U_{\mathrm{GEM}} = 50\,\mathrm{V}$ on the electrodes.
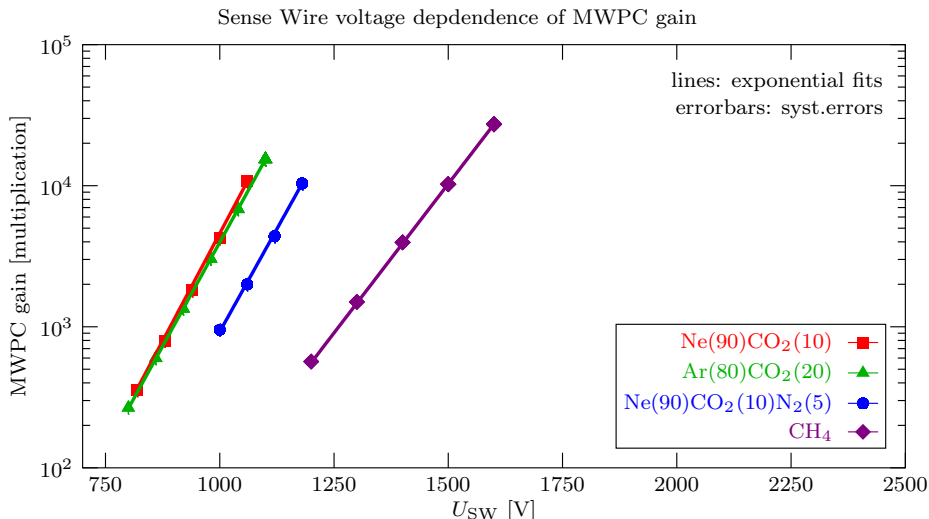

Figure 13. (Color online) The determined MWPC gain γ curves as a function of Sense Wire voltage U_{SW}, in various working gases. The shape of the curves were determined at a fixed large effective PE yield (≈ 1) and at fixed large GEM gain (≈ 50), using Sense Wire voltage scan. The normalization of the curves were done at large effective PE yield (≈ 1) and with transparent GEM setting (net effective gain ≈ 1), via Eq.(5.10).

6 Results on GEM response distributions

The measurement results of the 1-PE response analysis is shown in Fig. 15 and 16. In Fig. 15 the reconstructed net effective GEM multiplication distributions for single incoming electron, in different working gases and at various net effective gain settings are summarized. Fig. 16 shows the sigma-over-mean ratios, obtained via the simpler method of moment reconstruction. Both results show that in a given working gas the shape of the GEM multiplication distribution has very little gain dependence in the studied region of net
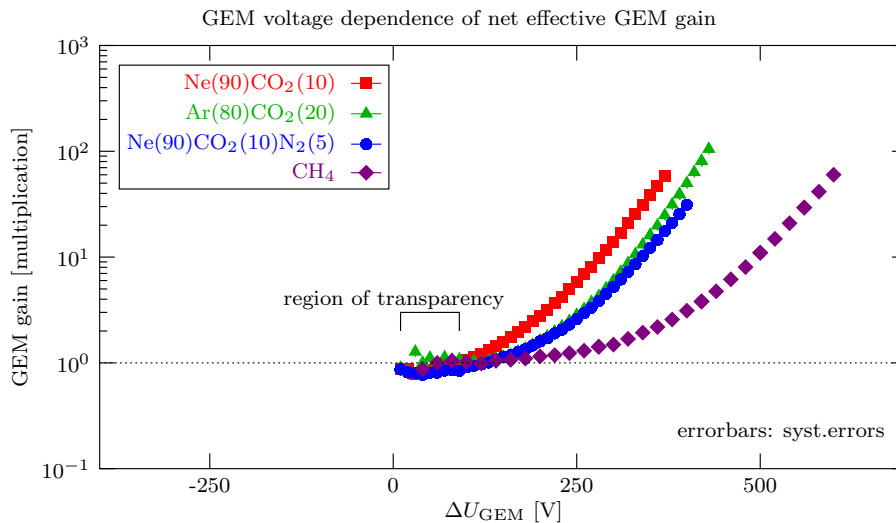
Figure 14. (Color online) The determined net effective GEM gain curves as a function of GEM voltage ΔU_{GEM}, in various working gases.

GEM effective gains, i.e. above about 15. On the other hand, there is a non-negligible working gas dependence of the multiplication distributions. In pure CH_4 the multiplication response is rather exponential-like, with a sigma-over-mean close to 1. In the mixture $Ar(80)CO_2(20)$ a substantial deviation from the exponential distribution at low amplitudes is observed, with a decreased sigma-over-mean ratio. The mixture $Ne(90)CO_2(10)N_2(5)$, to be used as working gas in the ALICE experiment [6], shows an even more suppressed yield of low amplitude GEM responses, resulting in an even smaller sigma-over-mean ratio. The mixture $Ne(90)CO_2(10)$ was seen to provide the best intrinsic response resolution, i.e. the smallest sigma-over-mean ratio.

The estimated net GEM effective gains carry about 10% systematic errors inherited from the MWPC gain curve normalization estimation via Eq.(5.10). That originates from the uncertainty of the true value of the sigma-over-mean ratio of the MWPC response distribution, estimated to be about at most 10% below the value 1, corresponding to idealized avalanche processes.

The raw data for the Fourier based Poisson compound decomposition of the 1-PE multiplication response distributions were obtained at large effective PE yield ν_{eff} of the order of 1 PE per pulse for an increased signal to noise ratio. The principle of that reconstruction was shown in Figs. 7,8,9 and the MWPC unfolding method was shown in Fig. 12. The systematic error of this analysis originates from the estimation accuracy of ν_{eff}, which is better than 5% in systematics, and that propagates directly into the shape accuracy of the reconstructed multiplication distributions.

For the determination of the intrinsic response resolution, i.e. of the sigma-over-mean ratio of GEM multiplication distribution could be performed both at the low PE yield ($\nu_{\mathrm{eff}} \approx 10^{-2}$) and large PE yield ($\nu_{\mathrm{eff}} \approx 1$) limit, using the formula Eq.(5.7). The systematic errors of the estimated effective PE yield ν_{eff} is smaller in the large ν_{eff} limit, since it can
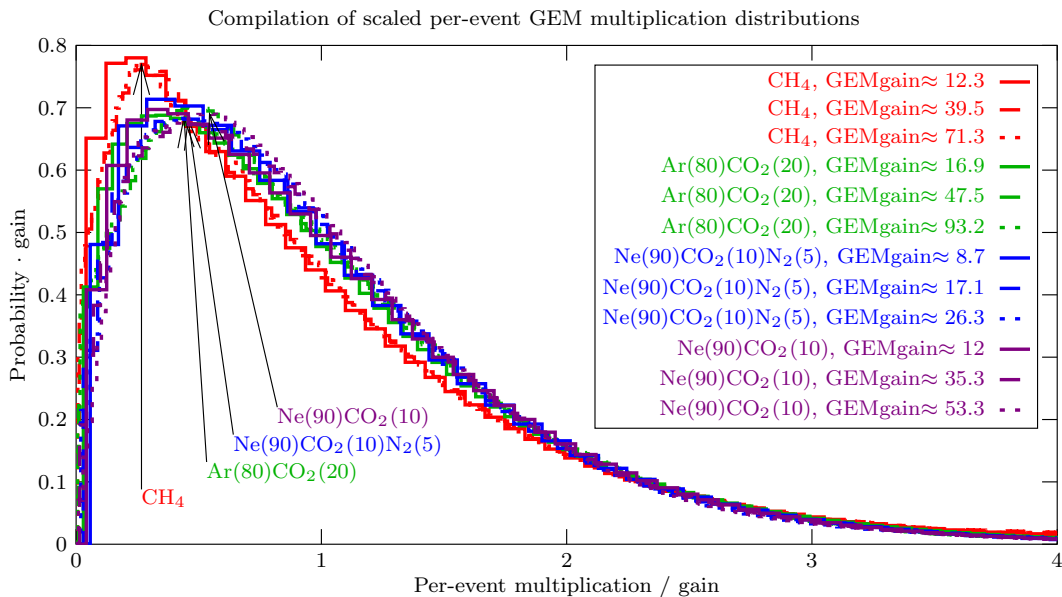
Figure 15. (Color online) Reconstructed shapes of the net effective 1-electron multiplication distribution in GEM avalanche processes in various working gases at various net GEM effective gains. In a given working gas, very little gain dependence of the response shapes is seen. On the other hand, there is a systematic shape difference in different working gases. The closest to exponential shape is seen in CH_4, whereas the most suppressed low amplitude region is observed in $Ne(90)CO_2(10)$ mixture.

be determined from the Fourier spectrum of the raw data in a relatively model independent way as was shown in Fig. 7. In the small PE yield limit the model fitting method as shown in Fig. 5 was used, for which an approximate model assumption is necessary for the shape of the 1-PE multiplication distribution, bringing in some extra systematics due to the slight effect of the extrapolation uncertainty. Therefore, the measurement results using the large PE yield raw data is more accurate, having about 2.5% systematic error, originating from the 5% systematics of the ν_{eff} determination.

7   Conclusions

In this paper a study on the single electron multiplication distribution in GEM foils has been presented. The experimental configuration based on photoelectron injection was outlined. The analysis methodologies for excluding detector effects such as multiple photoelectron contribution were detailed, and various cross-checks were shown. The multiplication distributions thus obtained show a deviation from exponential: low multiplication responses are suppressed in comparison to an exponential multiplication distribution of an idealized avalanche process. This improves the intrinsic detector resolution of GEM based detectors, the sigma-over-mean ratio, in comparison to traditional MWPC detectors, if significant loss of the initial electron is not present in the system. The shapes of the multiplication distributions were seen to have negligible gain dependence throughout the effective net gain
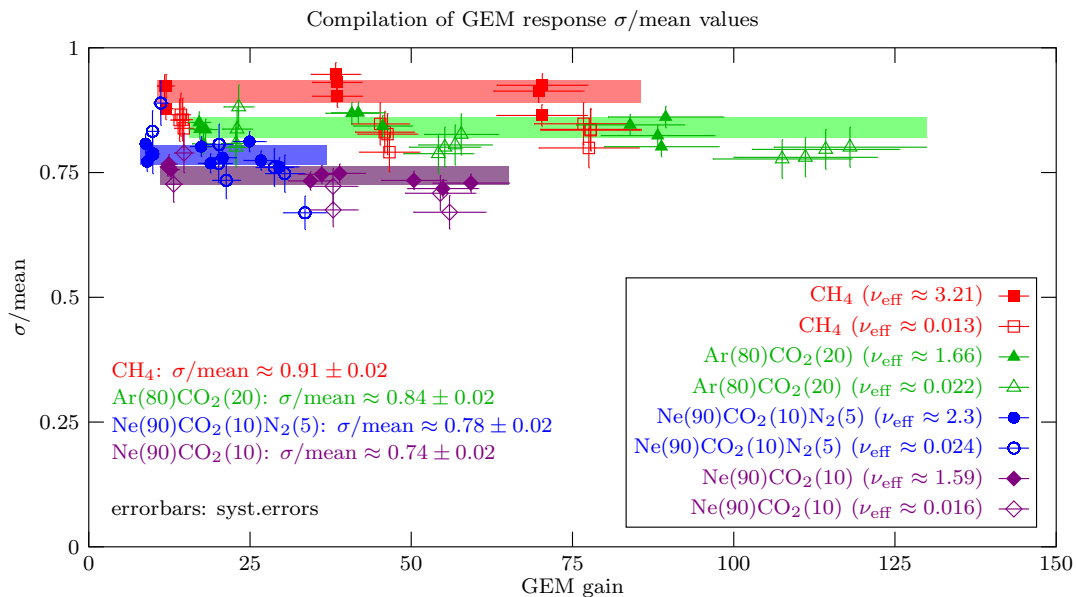
Figure 16. (Color online) The reconstructed sigma-over-mean ratios for the 1-electron multiplication distributions using the method of moments. In a given working gas, very little gain dependence of the sigma-over-mean ratio is seen. On the other hand, there is a systematic sigma-over-mean change between different working gases. The largest sigma-over-mean ratio was seen in CH_4, whereas the smallest was observed in $Ne(90)CO_2(10)$ mixture. The measurement results with low PE yield ($\nu_{\text{eff}} \approx 10^{-2}$) as well as with large PE yield ($\nu_{\text{eff}} \approx 1$) are also shown for consistency check purposes. The measurements with the large PE yield are more reliable due to their much smaller systematic uncertainty in terms of PE yield determination. The errorbars as well as the thickness of the colored bands indicate systematic errors.

range of about 15 to 100. On the other hand, a dependence on the working gas was observed. A sigma-over-mean ratio down to 0.75 was measured in neon-based working gases. That value is significantly lower than in case of traditional MWPC based multiplication processes, which are known to show a more exponential-like behavior.

Acknowledgements

References

[1] G. D. Alkhazov et al, *Nucl. Instr. Meth.* **75** (1969) 161.

[2] G. D. Alkhazov et al, *Nucl. Instr. Meth.* **89** (1970) 155.

[3] T. Zerguerras et al, *Nucl. Instr. Meth.* **A608** (2009) 397.

[4] T. Zerguerras, New results on gas gain fluctuations in a Micromegas detector (*Talk at RD51 Collab.Meeting, Zaragoza, 2013*) `https://indico.cern.ch/event/258852/session/1/` `contribution/122/material/slides/1.pdf`

[5] F. Sauli, *Nucl. Instr. Meth.* **A805** (2016) 2.

[6] B. Abelev et al (the ALICE Collaboration), Technical Design Report for the upgrade of the ALICE Time Projection Chamber, `CERN-LHCC-2013-020` (2013).

[7] Garfield++ `http://garfieldpp.web.cern.ch/garfieldpp`

[8] D. Varga, *Advances in High Energy Physics* **2016** (2016) 8561743.

[9] G. Hamar, D. Varga, *Nucl. Instr. Meth.* **A694** (2012) 16.

[10] D. Varga, G. Hamar, G. Kiss, *Nucl. Inst. Meth.* **A648** (2011) 163.

[11] D. Varga, G. Kiss, G. Hamar, G. Bencédi, *Nucl. Inst. Meth.* **A698** (2013) 11.

[12] B. Azmoun et al, Nuclear Science Symposium Conference Record vol. 6 (IEEE, 2006) pp 3847-3851.

[13] W. Feller, *An Introduction to Probability Theory and Its Applications* 3rd edn (New York: Wiley, 1968).

[14] F. A. Haight, *Handbook of the Poisson Distribution* (New York: Wiley, 1967).

[15] W. Blum, W. Riegler, L. Rolandi, *Particle Detection with Drift Chambers* (Berlin: Springer-Verlag, 2008).

[16] G. Arfken, Convolution theorem 15.5 *Mathematical Methods for Physicists* 3rd edn (Orlando, FL: Academic, 1985) pp 810-14.

[17] R. N. Bracewell, Convolution theorem *The Fourier Transform and Its Applications* 3rd edn (New York: McGraw-Hill, 1999) pp 108-12.

[18] W. Rudin, Theorem 9.6 *Real and Complex Analysis* 3rd edn (New York: McGraw-Hill, 1987) pp 182.

[19] The GNU Scientific Library `http://www.gnu.org/software/gsl`

[20] A. László, Convergence and error propagation results on a linear iterative unfolding method (*in review at SIAM JUQ, 2016*) [`arXiv:1404.2787`].

[21] A. László, The LibUnfold library `http://www.rmki.kfki.hu/~laszloa/downloads/` `libunfold.tar.gz`

[22] A. László, *J. Phys. Conf. Ser.* **368** (2012) 012043.